Composition and temperature of komatiite melts from Gorgona Island, Colombia, constrained from olivine-hosted melt inclusions

Vadim S. Kamenetsky[1]*, Andrey A. Gurenko[2], and Andrew C. Kerr[3]
[1]ARC Centre of Excellence in Ore Deposits and School of Earth Sciences, University of Tasmania, Hobart, Tasmania 7001, Australia
[2]Max-Planck-Institut für Chemie, Postfach 3060, 55020 Mainz, Germany, and Woods Hole Oceanographic Institution, Woods Hole, Massachusetts 02543, USA
[3]School of Earth and Ocean Sciences, Cardiff University, Park Place, Cardiff, Wales CF10 3YE, UK

ABSTRACT

Despite significant efforts in studying komatiites, their primary melt compositions and volatile abundances remain largely unknown because of significant alteration. Late Cretaceous komatiites of Gorgona Island, Colombia, are unambiguous samples of high-Mg melts derived from depleted mantle peridotite and are much fresher than most of their Archean counterparts. This work presents major, trace, and volatile element data for homogenized melt inclusions in olivine (forsterite, $Fo_{89.0–91.5}$) from the cumulate and upper sections of lava flows representing typical Gorgona Island komatiite (type G1). Major elements and lithophile trace elements of melt inclusions belong to a single fractionation series, which extends to the whole-rock komatiite compositions by addition of olivine. Melt inclusions are significantly enriched in volatile elements relative to elements of similar incompatibility (e.g., Cl/K 0.6–1.5; B/La 1.1–2.9; H_2O/Ce 600–4000). The melt inclusions have a primary melt composition of ~17 wt% MgO with a calculated anhydrous liquidus temperature of ~1390 °C. However, given the presence of 0.2–1.0 wt% H_2O, the initial crystallization temperature could be as low as 1330–1340 °C, but still higher than the temperature of common mid-ocean ridge magmas. The magmatic origin of volatiles in the komatiite melt has significant implications for composition and melting of the mantle source.

INTRODUCTION

Much debate about the nature of komatiitic magmas and their mantle sources has centered around mantle potential temperatures and the effects of volatile components (mainly H_2O) on reducing the solidus of depleted mantle peridotite (e.g., Arndt et al., 1998; Berry et al., 2008; Grove and Parman, 2004; Herzberg et al., 2007; Parman et al., 1997). Current estimates of crystallization temperatures are based on MgO contents in whole rocks, compositions of liquidus olivine, and thermodynamic modeling of the dry olivine-melt equilibrium. Estimates of original MgO abundances might be influenced by the accumulation of olivine in komatiitic flows and the effects of postmagmatic alteration and metamorphism. This, and uncertainties in the concentration of water in parental melts, may result in erroneous temperature calculations, which in turn can significantly affect petrological, geochemical, and geodynamic modeling of the mantle sources.

Magnesium and volatile abundances in the primary komatiite melts are the most critical parameters in these calculations and so should be quantified as accurately and as directly as possible. Unfortunately, quantification of the H_2O contents in the komatiitic melt is affected by indirect approaches, such as use of constant ratios of H_2O to lithophile elements of similar incompatibility (e.g., Ce; Herzberg et al., 2007) in support of anhydrous komatiite magmas, or water-bearing magmatic phases (e.g., amphibole; Echeverria and Aitken, 1986; Fiorentini et al., 2008; Stone et al., 1997) and specific pyroxene compositions (e.g., Parman et al., 1997) in conjunction with vesicularity of lavas and pyroclastic textures (e.g., Barley et al., 2000; Beresford et al., 2000; Capdevila et al., 1999; Dann, 2001; Echeverria and Aitken, 1986; Kerr et al., 1996) to advocate H_2O-rich komatiite magmas.

Although the melt inclusion approach is now being routinely used to assess the petrogenesis of many rock types and is particularly useful in deciphering the volatile budget of magmas (e.g., Danyushevsky et al., 2002b; Metrich and Wallace, 2008), the method has not been widely used to investigate the petrogenesis of komatiites, apart from a few studies on remarkably fresh Belingwe rocks (e.g., Berry et al., 2008; McDonough and Ireland, 1993; Shimizu et al., 2001). In part, this is because (1) komatiites are intrinsically altered rocks with a significant proportion of their phenocrystic olivine being fractured and replaced by serpentine, and (2) the melt inclusions, entrapped during rapid growth of the spinifex olivine, remained connected to the external melt (Fig. 1B). Here we present geochemical data on primary melt inclusions, hosted in nonspinifex olivine from the least altered komatiites from Gorgona Island, that demonstrate the potential of such studies in deciphering composition and temperature of komatiite parental melts.

GORGONA ISLAND KOMATIITES: OCCURRENCE AND SAMPLES

Gorgona Island, 50 km off the west coast of Colombia, is characterized by a wide range of igneous rocks (e.g., enriched to depleted basalts, picrite dikes and breccias, gabbros, wherlites, and dunites), and is best known for its ca. 90 Ma spinifex textured komatiites (see review in Kerr, 2005). The studied samples were collected from fresh coastal exposures of komatiites on the northeast side of the island (GOR94–17, GOR94–28, and GOR94–44 from Playa Pizarro and GOR94–3 and GOR94–4 from Punta Trinidad).

The essentially flat-lying Gorgona komatiite flows can be traced over distances of as much as 300 m and are interlayered with basaltic flows and sills. Komatiite flows are commonly layered, and vary in thickness from 1 to 3 m (Kerr, 2005). An upper polyhedrally jointed layer, 20–100 cm thick, containing skeletal olivine microphenocrysts (0.2–0.5 mm) in a very fine grained matrix, grades into a 10–40-cm-thick layer composed of fine random spinifex-textured skeletal olivine plates, set in a groundmass of feathery pyroxenes. Below this, the spinifex textured layer consists of hollow olivine megacrysts that range to 50 cm in length, and occasionally this is underlain by a thin layer (to 30 cm thick) of horizontally oriented, skeletal olivine plates as much as 10 cm long. Although some flows have a lower olivine cumulate layer, many flows do not. Where cumulate layers do exist they are generally thin (20–30 cm) and discontinuous, and represent no more than 30% of the flow. The cumulate olivine crystals are as large as 1 mm, have a predominant skeletal, but polyhedral habit, and are set in a groundmass of radiating needles of clinopyroxene, granular olivine, plagioclase laths, and Cr-spinel octrahedra (Figs. 1A, 1C, and 1D). Samples GOR94–3, GOR94–4, GOR94–17, and GOR94–44 are from the cumulate zone, whereas GOR94–28 (Fig. 1B) is from the jointed top of a flow. As noted by Kerr et al. (1996), several komatiite flows north of Punta Trinidad have vesicular zones as much as 15 cm thick near the center of the flow, between the main spinifex-textured layer and the horizontal spinifex layer. These prehnite-filled vesicles are large as 1 cm in diameter and

*E-mail: Dima.Kamenetsky@utas.edu.au.

© 2010 Geological Society of America. For permission to copy, contact Copyright Permissions, GSA, or editing@geosociety.org.

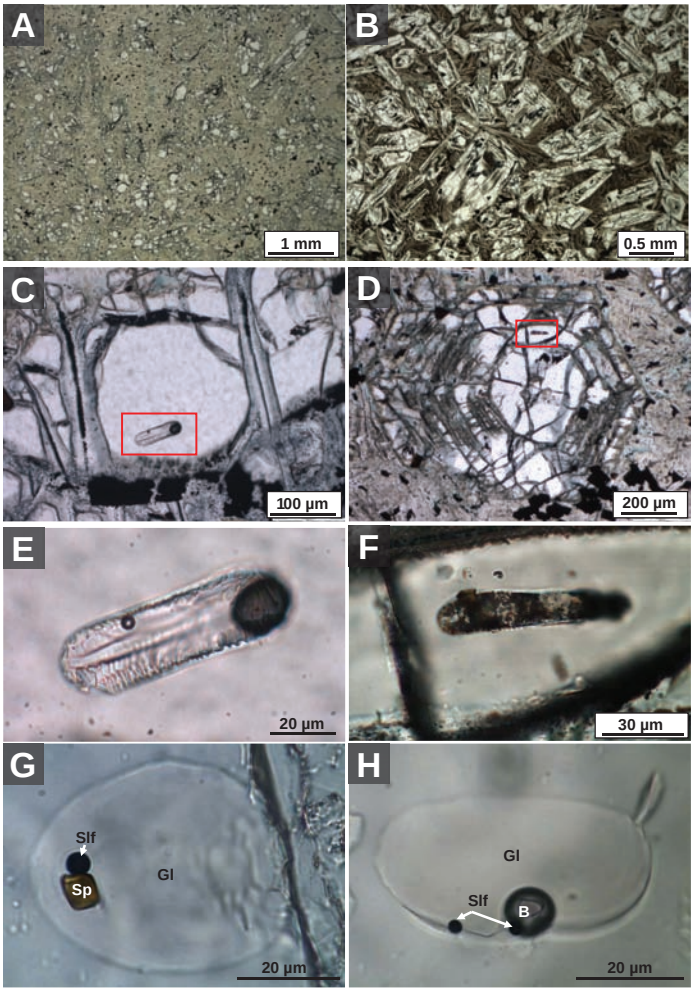

Figure 1. Host olivine and melt inclusions in Gorgona komatiites. A, D: Cumulate sample GOR94–44. B: Joint top flow sample GOR94–28. C: Cumulate sample GOR94–3. E, F: Unheated melt inclusions are enlargements of rectangular areas in C and D, respectively. G, H: Homogenized melt inclusions. Gl—glass; B—vapor bubble; Slf—sulfide globule; Sp—Cr-spinel.

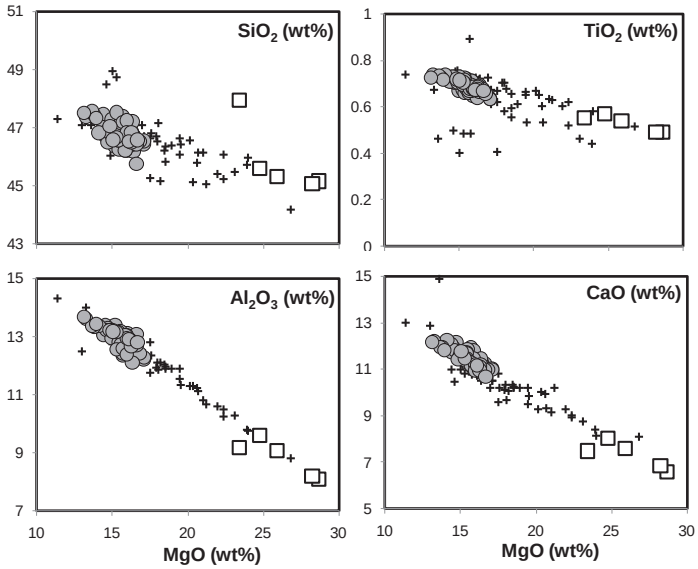

Figure 2. Compositions of Gorgona Island komatiites and basalts (crosses, literature data), studied komatiites (squares), and homogenized and recalculated melt inclusions (circles; Table DR3 [see footnote 1]). All compositions are normalized to 100 wt%.

locally constitute as much as 30% of the rock. Sample GOR94–17 was collected from the cumulate zone of a flow with a vesicular zone.

All studied samples have whole-rock major and trace element compositions typical of the Gorgona Island komatiites that are controlled by olivine fractionation and/or accumulation (Fig. 2; Table DR1 in the GSA Data Repository[1]).

OLIVINE AND CR-SPINEL

The olivine crystals in this study are fragmented by portions of melt entrapped during skeletal growth, fractured, and partially serpentinized along fractures and margins (Figs. 1A–1D). Only small fragments of entire crystals remain intact for analysis and melt inclusion studies (Figs. 1C–1F). Olivine, analyzed by electron microprobe (Table DR2) around spinel and melt inclusions, has limited compositional variations in terms of Fo content (89.0–91.5 mol%) and trace element abundances that reflect changes during fractionation from a single parental melt [e.g., increasing MnO (0.12–0.17 wt%) and CaO (0.31–0.34 wt%), and decreasing NiO (0.45–0.39 wt%) and Cr_2O_3 (0.15–0.09 wt%)]. Euhedral reddish-brown spinel is present as microphenocrysts and as inclusions in olivine. The spinel compositions belong to the low-Al end of the mid-oceanic ridge basalt (MORB) compositional array (Kamenetsky et al., 2001) in having high Mg# (65–75 wt%) and moderate Cr# (52–60 mol%) and TiO_2 contents (0.35–0.42 wt%). Both olivine and Cr-spinel compositions are comparable to those reported in other studies, and are among the most primitive found in Gorgona komatiites (Aitken and Echeverria, 1984; Dietrich et al., 1981; Echeverria, 1980).

OLIVINE-HOSTED MELT INCLUSIONS

The study of the melt inclusions in the Gorgona komatiites has presented a significant challenge due to the small size of host olivine fragments (Fig. 1). Melt inclusions, varying in size (to 60 µm) and shape (ovoid to tubular), appear as either clear glass with a shrinkage bubble or microcrystalline aggregates with several bubbles (Figs. 1E and 1F). Heating and quenching was used to convert the inclusions into glass. The temperature of complete melting was determined from several experiments with visual control. The olivine grains and a piece of graphite were wrapped in Pt foil, heated in a vertical furnace with a flow of pure Ar gas at 1275 °C for 2 min, and then quenched in water. The epoxy-mounted grains were polished to expose homogenized melt inclusions for in situ analysis by the microbeam techniques (Analytical Methods; see the Data Repository).

The rehomogenized inclusions are represented by a brownish glass, often with a vapor bubble (<2 vol%), a sulfide globule, and occasionally an accidently trapped Cr-spinel crystal of variable size (Figs. 1G and 1H). Sulfide globules are volumetrically proportional to the size of host glass, and thus represent a daughter phase that formed during cooling in relation to the so-called Fe loss process, caused by postentrapment crystallization and reequilibration with the host olivine (Danyushevsky et al., 2000, 2002b).

The Fe loss, found in all inclusions, is greater in more magnesian olivine from the slower cooled cumulate samples (to 5 wt% FeO). Thus, the measured melt compositions (Table DR2) were corrected to account

[1]GSA Data Repository item 2010279, analytical and calculation methods, and Tables DR1−DR3, is available online at www.geosociety.org/pubs/ft2010.htm, or on request from editing@geosociety.org or Documents Secretary, GSA, P.O. Box 9140, Boulder, CO 80301, USA.

for the Fe loss using the method by Danyushevsky et al. (2000) and recalculated to be in equilibrium with the host olivine applying the model of Ford et al. (1983) using PETROLOG software (Danyushevsky, 2001). Melt inclusion compositions show trends that are controlled by olivine fractionation from a single parental melt (from 17 to 13 wt% MgO for equilibrium olivine Fo 91.5–89.0 mol%, respectively) and consistent with the whole-rock compositions (Fig. 2; Tables DR1 and DR3).

Lithophile trace element compositions of melt inclusions are very homogeneous (Fig. 3) and resemble whole-rock compositions in having unfractionated heavy rare earth elements and progressive depletion in highly incompatible elements (e.g., Ba, Nb, K, La). In the overall smooth mantle-normalized trace element patterns of melt inclusions, the volatile elements, such as B, Cl, and H_2O, show strong positive anomalies relative to the lithophile elements of similar incompatibility (Fig. 3; Table DR2).

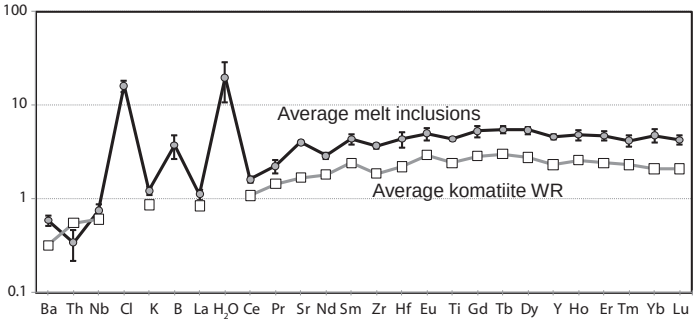

Figure 3. Pyrolite mantle-normalized (after McDonough and Sun, 1995) average trace element compositions of Gorgona komatiites (squares) and olivine-hosted melt inclusions (circles). Normalization values are 0.3 ppm B, 17 ppm Cl, and 300 ppm H_2O (based on H_2O/Ce = 180 and 1.675 ppm Ce). Observed variability is shown by bars. WR—whole rock.

DISCUSSION

Gorgona Komatiites—A Single Parental Melt

The compositions of the studied Gorgona komatiites and melt inclusions belong to the G1 magma type (Révillon et al., 2000). The melt inclusions are systematically lower in MgO, and higher in all elements incompatible with olivine, than most whole-rock compositions (Figs. 2 and 3). The observed compositional trends (Fig. 2) are controlled by the crystallization of olivine and Cr-spinel. The primary komatiite melt with ~17 wt% MgO can be identified from the melt inclusions hosted in the most primitive olivine 91.5 mol% Fo, or calculated from rock and/or melt inclusion compositions in equilibrium with such olivine by subtracting and/or adding the olivine component. Our estimate of MgO in the primary melt is 1–3 wt% lower than other calculations for Gorgona komatiites (e.g., ~18 wt% [Arndt et al., 1997; Kerr et al., 1996], ~19 wt% [Herzberg and O'Hara, 2002] and ~20 wt% [Aitken and Echeverria, 1984]). The uncertainties in calculated MgO depend on the olivine-melt equilibrium model and the melt oxidation state. The model by Ford et al. (1983), adopted here, has been tested and recommended for low-pressure liquidus calculations based on the comprehensive review of experimental data (Falloon et al., 2007).

Our melt inclusion study (Figs. 2 and 3) supports, at least with respect to the most common komatiite magma type found on the island (G1 after Révillon et al., 2000), the earlier conclusion that "…the Gorgona komatiites may have been derived from a single primary magma whose composition was subsequently modified by olivine fractionation/accumulation at shallow depths" (Aitken and Echeverria, 1984, p. 99).

Volatile Element Enrichment—A Magmatic or Contamination Signature?

Our study shows that major and trace element compositions of the olivine-hosted melt inclusions (Fig. 1) are representative of komatiitic parental melts (Figs. 2 and 3; Table DR3). Thus, the high volatile abundances in the melt inclusions (Fig. 3; averaged ratios H_2O/Ce = 2150 ± 950, Cl/K_2O = 0.76 ± 0.14, B/La = 1.62 ± 0.46), without notable variations in major and trace elements at a given olivine composition, may also reflect primary magmatic values in the Gorgona komatiite. If magmatic in origin, the high and variable H_2O contents in the Gorgona melt inclusions (0.2–1.0 wt%) are of particular relevance to the petrogenesis of komatiites (e.g., Arndt et al., 1998; Berry et al., 2008; Grove and Parman, 2004; Herzberg et al., 2007; Parman et al., 1997). Relatively high H_2O abundances in melt inclusions have also been reported for the Belingwe komatiites in Zimbabwe (0.18–0.26 wt%—Danyushevsky et al., 2002a; 1.1 and 1.7 wt%—Shimizu et al., 2001; 0.4–0.6 wt%—Kent et al., 2009). It is noteworthy that the Belingwe melt inclusions are also enriched in Cl (500–700 ppm, Cl/K_2O ~0.8–1.5; Kent et al., 2009). If the postentrapment diffusion of hydrogen into melt inclusions (e.g., Portnyagin et al., 2008) is excluded, based on enrichment in other volatile elements, which diffuse much more slowly, then the original H_2O in the primary melt could have been even higher (Danyushevsky et al., 2002a). In other words, the komatiitic melts possibly underwent strong H_2O degassing on ascent prior to crystallization of olivine, if the melt was overheated as a result of adiabatic decompression (Danyushevsky et al., 2002b). However, whether the primary melt contained much more than 1 wt% H_2O is not critical for calculating liquidus temperature, as temperature dependence on H_2O is strongly nonlinear (Falloon and Danyushevsky, 2000).

Enrichment in volatile elements CO_2, F, H_2O, and Cl has been reported for the melt inclusions in chromite grains from beach sands on Gorgona Island (Shimizu et al., 2009). The high and variable H_2O/Ce and Cl/K_2O (307 ± 198 and 1.07 ± 0.52, respectively) in melt inclusions hosted by Cr-spinel, which is compositionally similar to Cr-spinel in our samples (i.e., komatiitic) were assigned to seawater and/or brine assimilation by the magma at upper mantle depths (Shimizu et al., 2009). Although Shimizu et al. (2009) rejected a magmatic origin of H_2O and Cl in the Gorgona komatiite, they argued that the concomitant enrichment of the melt in CO_2 and F was inherited from the subduction-modified mantle source. It seems unrealistic that the magma enrichment in the volatile elements, including boron measured in our study, can be attributed to different sources and processes. We thus believe that the enrichment of the studied melt inclusions in the volatile elements is magmatic in origin.

Liquidus Temperature of Komatiite

Modeling shows that the slightly lower (than previously calculated) MgO content of the Gorgona komatiite primary melt in equilibrium with the most primitive olivine Fo 91.5 results in a dry liquidus temperature of 1387 °C. This calculated liquidus temperature is 50–60 °C lower when the magma contains small amounts of H_2O (0.3–0.6 wt%). However, if the primary komatiite melt was anhydrous and contaminated by water during ascent, it had to cool and/or degas significantly prior to crystallization of olivine. Whatever the origin of H_2O in the Gorgona komatiite melt, the initial crystallization temperature of 1330–1340 °C is at the upper limit of such temperatures reported for rare samples with primitive olivine (>91 mol% Fo) from the mid-oceanic rifts (e.g., Falloon et al., 2007). However, despite close geochemical and isotopic similarities between the Gorgona komatiite and common MORB, Gorgona komatiites are more MgO rich (by at least 3–4 wt%), and thus hotter than MORB. Consequently, this requires a mantle source, which is depleted yet different from the source of common MORB. The elevated magmatic H_2O in the komatiite primary melt points to hydration of the mantle source; however, the absence of a negative Nb anomaly (Fig. 3)

would seem to preclude a subduction-related origin for this H_2O, and so further work is required to assess the source of these volatiles and provide constraints for the geodynamic context and melting models.

ACKNOWLEDGMENTS

The thin sections and olivine separates were provided by Bill McDonough. We thank Alex Sobolev for analyzing a subset of selected inclusions by secondary ion mass spectrometry (SIMS) for H_2O and for fruitful discussions. Comments from K. Putirka, four anonymous reviewers, A.P. Barth, and W.J. Collins helped to clarify the text and refine several conclusions. This research was supported by Research Fellowship and Discovery grants (Australian Research Council) and the F.W. Bessel Award (A. von Humboldt Foundation, Germany) to Kamenetsky, and the Wolfgang Paul Award (A. von Humboldt Foundation, Germany) to A. Sobolev.

REFERENCES CITED

Aitken, B.G., and Echeverria, L.M., 1984, Petrology and geochemistry of komatiites and tholeiites from Gorgona Island, Colombia: Contributions to Mineralogy and Petrology, v. 86, p. 94–105, doi: 10.1007/BF00373714.

Arndt, N.T., Kerr, A.C., and Tarney, J., 1997, Dynamic melting in plume heads: The formation of Gorgona komatiites and basalts: Earth and Planetary Science Letters, v. 146, p. 289–301, doi: 10.1016/S0012-821X(96)00219-1.

Arndt, N., Ginibre, C., Chauvel, C., Albarède, F., Cheadle, M., Herzberg, C., Jenner, G., and Lahaye, Y., 1998, Were komatiites wet?: Geology, v. 26, p. 739–742, doi: 10.1130/0091-7613(1998)026<0739:WKW>2.3.CO;2.

Barley, M.E., Kerrich, R., Reudavy, I., and Xie, Q., 2000, Late Archaean Ti-rich, Al-depleted komatiites and komaiitic volcaniclastic rocks from the Murchison Terrane in Western Australia: Australian Journal of Earth Sciences, v. 47, p. 873–883, doi: 10.1046/j.1440-0952.2000.00820.x.

Beresford, S.W., Cas, R.A.F., Lambert, D.D., and Stone, W.E., 2000, Vesicles in thick komatiite lava flows, Kambalda, Western Australia: Geological Society of London Journal, v. 157, p. 11–14.

Berry, A.J., Danyushevsky, L.V., O'Neill, H.S.C., Newville, M., and Sutton, S.R., 2008, Oxidation state of iron in komatiitic melt inclusions indicates hot Archaean mantle: Nature, v. 455, p. 960–963, doi: 10.1038/nature07377.

Capdevila, R., Arndt, N., Letendre, J., and Sauvage, J.F., 1999, Diamonds in volcaniclastic komatiite from French Guiana: Nature, v. 399, p. 456–458, doi: 10.1038/20911.

Dann, J.C., 2001, Vesicular komatiites, 3.5 Ga Komati Formation, Barberton Greenstone Belt, South Africa: Inflation of submarine lavas and origin of spinifex zones: Bulletin of Volcanology, v. 63, p. 462–481, doi: 10.1007/s004450100164.

Danyushevsky, L.V., 2001, The effect of small amounts of H_2O on crystallisation of mid-ocean ridge and backarc basin magmas: Journal of Volcanology and Geothermal Research, v. 110, p. 265–280, doi: 10.1016/S0377-0273(01)00213-X.

Danyushevsky, L.V., Della-Pasqua, F.N., and Sokolov, S., 2000, Re-equilibration of melt inclusions trapped by magnesian olivine phenocrysts from subduction-related magmas: Petrological implications: Contributions to Mineralogy and Petrology, v. 138, p. 68–83, doi: 10.1007/PL00007664.

Danyushevsky, L.V., Gee, M.A.M., Nisbet, E.G., and Cheadle, M.J., 2002a, Olivine-hosted melt inclusions in Belingwe komatiites: Implications for cooling history, parental magma composition and its H_2O content: Geochimica et Cosmochimica Acta, v. 66, no. 15A, supplement, p. A168.

Danyushevsky, L.V., McNeill, A.W., and Sobolev, A.V., 2002b, Experimental and petrological studies of melt inclusions in phenocrysts from mantle-derived magmas: An overview of techniques, advantages and complications: Chemical Geology, v. 183, p. 5–24, doi: 10.1016/S0009-2541(01)00369-2.

Dietrich, V.J., Gansser, A., Sommerauer, J., and Cameron, W.E., 1981, Palaeogene komatiites from Gorgona Island, East Pacific—A primary magma for ocean floor basalts?: Geochemical Journal, v. 15, p. 141–161.

Echeverria, L.M., 1980, Tertiary or Mesozoic komatiites from Gorgona island, Colombia: Field relations and geochemistry: Contributions to Mineralogy and Petrology, v. 73, p. 253–266, doi: 10.1007/BF00381444.

Echeverria, L.M., and Aitken, B.G., 1986, Pyroclastic rocks: Another manifestation of ultramafic volcanism on Gorgona Island, Colombia: Contributions to Mineralogy and Petrology, v. 92, p. 428–436, doi: 10.1007/BF00374425.

Falloon, T.J., and Danyushevsky, L.V., 2000, Melting of refractory mantle at 1.5, 2 and 2.5 GPa under anhydrous and H_2O-undersaturated conditions: Implications for the petrogenesis of high-Ca boninites and the influence of subduction components on mantle melting: Journal of Petrology, v. 41, p. 257–283, doi: 10.1093/petrology/41.2.257.

Falloon, T.J., Danyushevsky, L.V., Ariskin, A., Green, D.H., and Ford, C.E., 2007, The application of olivine geothermometry to infer crystallization temperatures of parental liquids: Implications for the temperature of MORB magmas: Chemical Geology, v. 241, p. 207–233, doi: 10.1016/j.chemgeo.2007.01.015.

Fiorentini, M.L., Beresford, S.W., Deloule, E., Hanski, E., Stone, W.E., and Pearson, N.J., 2008, The role of mantle-derived volatiles in the petrogenesis of Palaeoproterozoic ferropicrites in the Pechenga Greenstone Belt, northwestern Russia: Insights from in-situ microbeam and nanobeam analysis of hydromagmatic amphibole: Earth and Planetary Science Letters, v. 268, p. 2–14, doi: 10.1016/j.epsl.2007.12.018.

Ford, C.E., Russel, D.G., Craven, J.A., and Fisk, M.R., 1983, Olivine-liquid equilibria: Temperature, pressure and composition dependence of the crystal/liquid cation partition coefficients for Mg, Fe^{2+}: Ca and Mn: Journal of Petrology, v. 24, p. 256–265.

Grove, T.L., and Parman, S.W., 2004, Thermal evolution of the Earth as recorded by komatiites: Earth and Planetary Science Letters, v. 219, p. 173–187, doi: 10.1016/S0012-821X(04)00002-0.

Herzberg, C., and O'Hara, M.J., 2002, Plume-associated ultramafic magmas of Phanerozoic age: Journal of Petrology, v. 43, p. 1857–1883, doi: 10.1093/petrology/43.10.1857.

Herzberg, C., Asimow, P.D., Arndt, N., Niu, Y., Lesher, C.M., Fitton, J.G., Cheadle, M.J., and Saunders, A.D., 2007, Temperatures in ambient mantle and plumes: Constraints from basalts, picrites, and komatiites: Geochemistry Geophysics Geosystems, v. 8, Q02006, doi: 10.1029/2006GC001390.

Kamenetsky, V.S., Crawford, A.J., and Meffre, S., 2001, Factors controlling chemistry of magmatic spinel: An empirical study of associated olivine, Cr-spinel and melt inclusions from primitive rocks: Journal of Petrology, v. 42, p. 655–671, doi: 10.1093/petrology/42.4.655.

Kent, A.J.R., Hauri, E., Woodhead, J., and Hergt, J.M., 2009, Volatile contents of Belingewe komatiites: Mantle volatile contents and the effects of degassing: Geochimica et Cosmochimica Acta, supplement, v. 73, p. A640.

Kerr, A.C., 2005, La Isla de Gorgona, Colombia: A petrological enigma?: Lithos, v. 84, p. 77–101, doi: 10.1016/j.lithos.2005.02.006.

Kerr, A.C., Marriner, G.F., Arndt, N.T., Tarney, J., Nivia, A., Saunders, A.D., and Duncan, R.A., 1996, The petrogenesis of Gorgona komatiites, picrites and basalts: New field, petrographic and geochemical constraints: Lithos, v. 37, p. 245–260, doi: 10.1016/0024-4937(95)00039-9.

McDonough, W.F., and Ireland, T.R., 1993, Intraplate origin of komatiites inferred from trace elements in glass inclusions: Nature, v. 365, p. 432–434, doi: 10.1038/365432a0.

McDonough, W.F., and Sun, S.-s., 1995, The composition of the Earth: Chemical Geology, v. 120, p. 223–253, doi: 10.1016/0009-2541(94)00140-4.

Metrich, N., and Wallace, P.J., 2008, Volatile abundances in basaltic magmas and their degassing paths tracked by melt inclusions: Reviews in Mineralogy and Geochemistry, v. 69, p. 363–402, doi: 10.2138/rmg.2008.69.10.

Parman, S.W., Dann, J.C., Grove, T.L., and de Wit, M.J., 1997, Emplacement conditions of komatiite magmas from the 3.49 Ga Komati Formation, Barberton Greenstone Belt, South Africa: Earth and Planetary Science Letters, v. 150, p. 303–323, doi: 10.1016/S0012-821X(97)00104-0.

Portnyagin, M., Almeev, R., Matveev, S., and Holtz, F., 2008, Experimental evidence for rapid water exchange between melt inclusions in olivine and host magma: Earth and Planetary Science Letters, v. 272, p. 541–552, doi: 10.1016/j.epsl.2008.05.020.

Révillon, S., Arndt, N.T., Chauvel, C., and Hallot, E., 2000, Geochemical study of ultramafic volcanic and plutonic rocks from Gorgona Island, Colombia: The plumbing system of an oceanic plateau: Journal of Petrology, v. 41, p. 1127–1153, doi: 10.1093/petrology/41.7.1127.

Shimizu, K., Komiya, T., Hirose, K., Shimizu, N., and Maruyama, S., 2001, Cr-spinel, an excellent micro-container for retaining primitive melts—Implications for a hydrous plume origin for komatiites: Earth and Planetary Science Letters, v. 189, p. 177–188, doi: 10.1016/S0012-821X(01)00359-4.

Shimizu, K., Shimizu, N., Komiya, T., Suzuki, K., Maruyama, S., and Tatsumi, Y., 2009, CO_2-rich komatiitic melt inclusions in Cr-spinels within beach sand from Gorgona Island, Colombia: Earth and Planetary Science Letters, v. 288, p. 33–43, doi: 10.1016/j.epsl.2009.09.005.

Stone, W.E., Deloule, E., Larson, M.S., and Lesher, C.M., 1997, Evidence for hydrous high-MgO melts in the Precambrian: Geology, v. 25, p. 143–146, doi: 10.1130/0091-7613(1997)025<0143:EFHHMM>2.3.CO;2.

Manuscript received 21 February 2010
Revised manuscript received 8 June 2010
Manuscript accepted 20 June 2010

Printed in USA

GSA Data Repository item 2010279

Composition and temperature of komatiite melts from Gorgona Island constrained from olivine-hosted melt inclusions

Vadim S. Kamenetsky, Andrey A. Gurenko, Andrew C. Kerr

Analytical Methods

Electron microprobe

Major elements in minerals and glasses were analyzed using the JEOL Superprobe JXA-8200 electron microprobe (Max Planck Institute for Chemistry, Mainz, Germany). We applied 15 kV accelerating voltage, 12 nA electron beam current and defocused to 5 μm size beam for analyses of host matrix glasses and olivine-hosted glass inclusions. The 20 kV and 20 nA primary beam was applied for analyses of olivine and spinel. Peak counting times on major elements were 60 s and 30 s of background. Standard built-in ZAF correction routine was used. Sulfur and chlorine were analysed at the same analytical conditions as other major elements in glasses. At these conditions, the detection limit for S was around 200–250 ppm. A set of reference materials (i.e. natural and synthetic oxides, minerals and glasses; Micro-Analysis Consultants Ltd, Cambridgeshire, UK) and the Smithsonian Institution standard set for electron microprobe analysis (Jarosewich et al., 1980) were used for routine calibration and instrument stability monitoring. Typical analytical uncertainties (2RSD = 2σ relative standard deviation) are 1.5–3.0% for SiO_2, Al_2O_3, FeO, MgO, CaO, TiO_2; 4-6% for Na_2O, 10% for K_2O, 15% for P_2O_5, and 30% for MnO. As a monitor sample for S and Cl measurements, we also used the USNM 111240/52 VG-2 basaltic glass (recommended values of 0.134–0.137 wt% S; (Dixon et al., 1991; Thordarson et al., 1996); 0.030 wt% Cl, N. Metrich, personal communication, 2003). The concentrations of 0.140 ± 0.023 wt% S and 0.029 ± 0.007 wt% Cl (±2σ SD = 2-sigma standard deviation, N = 37) were obtained during this study.

Ion microprobe

Glass inclusions were analyzed for H_2O, B, Cl and trace elements (REE, Nb, Th, Sr, Y, Zr, V and Cr) using the Cameca IMS 3f instrument at the MPI in Mainz. For H_2O, B and Cl analyses, conditions were similar to those described by (Chaussidon and Libourel, 1993; Sobolev and Chaussidon, 1996), with 12.5 kV accelerating voltage for the $^{16}O^-$ primary beam, 4.5 kV secondary accelerating voltage, –80 V offset and $M/\Delta M \approx 300$. The energy slit was centered and opened to 25 V. A 150 μm contrast aperture and a 750 μm field aperture were used. Analyses were performed in three blocks of 6 cycles over the masses ^{1}H, ^{11}B, ^{30}Si, ^{35}Cl and ^{47}Ti, counted during 4 s, 6 s, 2 s, 6 s and 2 s, respectively. Titanium was monitored to detect and, if necessary, correct for overlap with host minerals in the case of small (<40 μm) inclusions. A set of natural and synthetic glasses with water concentrations ranging from 0.1 to 2.1 wt.% H_2O and 14 to 1920 ppm B was used for calibration. The

olivine host grains were repeatedly analyzed throughout each session to monitor the H_2O background level, and inclusion analyses were started when H_2O concentration measured on olivine was equivalent to, or lower than, 0.03 wt%. The external precision, assessed from multiple measurements of reference glasses, was better than 10 rel%.
The analysis of trace elements employed similar instrument settings as for H_2O, except that a larger field aperture (1800 μm) was used. Each analysis consisted of 5 sequential scans of the masses ^{16}O, ^{30}Si, ^{35}Cl, ^{39}K, ^{44}Ca, ^{47}Ti, ^{51}V, ^{52}Cr, ^{88}Sr, ^{89}Y, ^{90}Zr, ^{93}Nb, then the REE masses from 133 to 180 and finally mass ^{232}Th. The remaining oxide interferences, e.g., light rare earth element (LREE) oxides interfering with heavy rare earth elements (HREE) were corrected by peak deconvolution (Fahey et al., 1987; Zinner and Crozaz, 1986). Relative sensitivity factors were determined from analyses of basaltic reference glasses (Jochum et al., 2000). Instrument drift was controlled and correction applied using daily replicate analyses of KL2-G reference glass. The obtained analytical error was better than 10% relative for all elements except Gd, Tm, Lu, Hf and Th whose uncertainties range between 11 and 30% relative.

Laser ablation ICP-MS
Trace element concentrations in the selected large (>40 μm) melt inclusions were analyzed with the single collector sector-field ICP-MS Element 2 equipped with the New Wave Research UP213 Nd-YAG (213 nm) laser at Max Planck Institute for Chemistry (Mainz, Germany). Analyses were performed in an Ar atmosphere by ablating 40 μm-diameter spots at a rate of 5 shots/sec using laser power of ~12 J/cm^2. The instrument was optimized for sensitivity on mid- to high-mass isotopes (in the range 80-240 a.m.u.) and for minimal molecular oxide species (i.e., $^{232}Th^{16}O/^{232}Th < 0.2\%$) and doubly-charges ion species (i.e., $^{140}Ce^{++}/^{140}Ce^{+} < 0.3\%$) production. The analysis time for each sample was 50-90 seconds, comprising a 30 second measurement of background (laser off) and a 20-60 second analysis (depending on inclusion's thickness) with laser on. Instrument calibration and stability monitoring was performed by ablating the NIST612 and KL2-G glass standards. Data reduction was undertaken according to standard methods ((Longerich et al., 1996) using the NIST612 glass (Pearce et al., 1997) as a primary reference material and KL2-G (Jochum et al., 2000) as the internal standard. The intensity of peacks were normalized to ^{43}Ca (Ca analysed by EMPA) The KL2-G reference glass (Jochum et al., 2000) glass was repeatedly analysed throughout analytical sessions and was used as a secondary reference material.

Table DR1. Compositions of studied komatiites from Gorgona Island, Columbia

Sample	GOR94-3	GOR94-4	GOR94-17	GOR94-28	GOR94-44
Type	cumulate	cumulate	cumulate	joint top	cumulate
SiO_2	45.06	44.88	47.80	44.38	45.53
TiO_2	0.49	0.49	0.55	0.53	0.57
Al_2O_3	8.07	8.15	9.15	8.89	9.59
Fe_2O_3	11.56	11.68	11.82	11.72	11.81
MnO	0.17	0.17	0.17	0.17	0.18
MgO	28.61	28.12	23.36	25.36	24.74
CaO	6.56	6.82	7.46	7.42	8.02
Na_2O	0.31	0.33	0.51	0.51	0.51
K_2O	0.05	0.02	0.01	0.03	0.02
P_2O_5	0.04	0.04	0.04	0.04	0.04
Total	100.90	100.69	100.87	99.05	101.02
LOI	3.69	3.32	2.36	1.98	2.43
Ba, ppm	3.170	1.718	1.831	2.467	2.048
Co, ppm	85.6	90.4	88.4	87.3	84.4
Cr, ppm					
Cu, ppm	91	90	95	91	96
Ga, ppm	10	9	10	10	10
Nb, ppm	0.33	0.52	0.51	0.42	0.40
Ni, ppm	1018	1228	935	1082	1050
Rb, ppm	0.87	0.60	0.65	0.80	0.64
Sc, ppm	32	29	34	32	33
Sr, ppm	36	30	37	38	37
Th, ppm	0.04	0.05	0.06	0.04	0.04
V, ppm	186	163	190	180	186
Y, ppm	10	10	11	11	11
Zn, ppm	70	66	69	68	67
Zr, ppm	21	20	22	21	22
La, ppm	0.60	0.56	0.61	0.57	0.57
Ce, ppm	1.96	1.83	2.03	1.91	1.93
Pr, ppm	0.42	0.37	0.42	0.40	0.40
Nd, ppm	2.58	2.22	2.57	2.44	2.50
Sm, ppm	1.11	0.97	1.13	1.07	1.10
Eu, ppm	0.52	0.45	0.52	0.50	0.51
Gd, ppm	1.77	1.52	1.79	1.72	1.76
Tb, ppm	0.34	0.29	0.34	0.32	0.33
Dy, ppm	2.11	1.83	2.14	2.05	2.09
Ho, ppm	0.44	0.38	0.45	0.43	0.43
Er, ppm	1.20	1.05	1.21	1.16	1.19
Tm, ppm	0.18	0.16	0.18	0.17	0.18
Yb, ppm	1.06	0.94	1.08	1.04	1.05

Lu, ppm	0.16	0.14	0.16	0.15	0.16
Hf, ppm	0.69	0.63	0.72	0.69	0.69
Th, ppm	0.04	0.05	0.06	0.04	0.04
U, ppm	0.01	0.01	0.01	0.01	0.01

Table DR2. Representative compositions of homogenised melt inclusions and their host olivine

Grain No	m1 94-28-1	m1 94-28-3mi1	m1 94-28-9	m2 94-17-11	m2 94-17-13	m3 94-4-20	m3 94-4-21	m3 94-44-24	m3 94-44-27	m1 94-28-2	m1 94-28-8a	m2 94-17-16	m4 94-3_30a	m4 94-3-32
Host olivine														
SiO_2	40.35	40.66	40.40	40.80	40.74	40.34	40.28	40.68	40.69	41.34	40.22	40.42	40.84	41.02
FeO	9.21	8.90	8.95	9.72	9.54	9.37	9.03	8.65	8.88	9.02	8.97	10.08	8.48	9.18
MnO	0.15	0.15	0.14	0.17	0.13	0.14	0.16	0.12	0.14	0.15	0.14	0.17	0.12	0.15
MgO	49.01	49.48	48.91	49.06	49.19	48.81	48.88	49.45	49.44	50.02	48.56	48.36	49.99	49.71
CaO	0.32	0.32	0.32	0.33	0.33	0.32	0.32	0.32	0.31	0.33	0.32	0.34	0.31	0.34
NiO	0.43	0.44	0.43	0.40	0.41	0.42	0.44	0.44	0.44	0.44	0.44	0.40	0.44	0.45
Cr_2O_3	0.11	0.12	0.14	0.10	0.12	0.12	0.11	0.12	0.11	0.13	0.14	0.11	0.12	0.13
Total	99.56	100.07	99.29	100.57	100.46	99.52	99.21	99.78	100.00	101.43	98.79	99.87	100.31	100.98
Fo, mol%	90.5	90.8	90.7	90.0	90.2	90.3	90.6	91.1	90.9	90.8	90.6	89.5	91.3	90.6
Heated Melt Inclusions														
SiO_2	49.42	48.55	48.37	48.61	48.14	49.02	49.16	48.94	49.08	47.98	48.84	49.11	48.25	48.43
TiO_2	0.95	0.86	0.87	0.87	0.86	0.85	0.87	0.87	0.85	0.88	0.88	0.84	0.85	0.85
Al_2O_3	17.17	16.12	15.79	15.68	15.60	15.58	15.91	15.27	15.50	16.11	16.01	15.46	15.90	15.85
FeO	7.15	8.37	8.90	6.62	7.11	6.48	6.23	6.57	6.56	7.94	8.40	7.57	6.14	6.91
MnO	0.11	0.18	0.13	0.12	0.15	0.09	0.09	0.08	0.11	0.16	0.14	0.15	0.13	0.13
MgO	8.39	9.92	10.06	10.39	10.76	11.03	10.76	10.31	10.43	9.73	9.66	10.95	11.70	11.45
CaO	15.00	14.07	14.13	14.36	13.88	13.89	14.17	14.07	13.95	14.62	14.37	13.79	13.64	13.75
Na_2O	2.12	1.98	1.85	1.79	1.93	1.80	1.85	1.79	1.79	1.96	1.88	1.84	1.92	1.95
K_2O	0.039	0.039	0.040	0.034	0.034	0.035	0.044	0.041	0.039	0.037	0.038	0.032	0.044	0.030
P_2O_5	0.070	0.062	0.056	0.044	0.052	0.058	0.061	0.051	0.046	0.061	0.057	0.054	0.046	0.054
S	0.071	0.073	0.076	0.052	0.056	0.056	0.056	0.052	0.059	0.077	0.072	0.064	0.052	0.068
Cl	0.029	0.030	0.029	0.026	0.025	0.029	0.025	0.026	0.026	0.028	0.031	0.022	0.023	0.025
Total	100.52	100.24	100.31	98.62	98.60	98.92	99.22	98.08	98.44	99.58	100.39	99.88	98.69	99.49

H2O wt%			0.18	0.73	0.44	1.03	0.59					0.64	0.44	0.27
Cl, ppm	285	300	272	236	254	296	277	263	257	280	313	273	205	184
B, ppm	*0.61*	2.02	0.95	1.10	1.07	1.09	1.10	1.48	0.88	1.63	0.81	0.93	1.03	1.01
K, ppm		321	288	246	265	299	308	343	327	307	313	290	334	270
Ti, ppm		5333	5395	5120	5198	5357	5266	5022	5130	5413	5313	5097	5081	5369
V, ppm			435	369	388	453	412					397	405	406
Cr, ppm			401	751	444	736	579					484	686	706
Sr, ppm		83.3	82.3	75.2	75.0	82.2	80.2	78.1	73.7	86.4	86.8	75.0	77.0	79.2
Y, ppm		19.9	19.4	18.4	18.7	18.6	19.6	19.5	18.3	22.0	21.5	19.4	19.8	19.6
Zr, ppm		40.9	40.4	36.5	37.0	38.2	39.2	37.1	35.9	42.3	41.3	35.7	37.9	39.1
Nb, ppm		0.53	0.44	0.60		0.48	0.51		0.57	0.53	0.50	0.48	0.49	0.52
Ba, ppm		4.0	3.9	4.0	4.3	4.5	4.3	4.4	3.4	3.3	3.5	3.4	3.7	4.3
La, ppm		0.79	0.73	0.77	0.77	0.69	0.71	0.77	0.59	0.81	0.77	0.61	0.77	0.77
Ce, ppm		2.72	2.94	2.81	2.47	2.65	2.87	2.54	2.38	2.82	2.70	2.80	2.71	2.70
Pr, ppm		0.50	0.70	0.57	0.60	0.64	0.56	0.52		0.67	0.51	0.55	0.59	0.55
Nd, ppm		3.61	3.61	3.84	3.72	3.46	3.46	3.89	3.45	3.81	3.43	3.50	3.52	3.40
Sm, ppm		1.44	1.88	1.68	1.62	1.89	1.80	1.62	1.60	2.18	2.34	1.64	1.92	1.68
Eu, ppm		1.03	0.83	0.84	0.72	0.80	0.85	0.62	0.82	0.96	0.78	0.69	0.63	0.71
Gd, ppm		2.93	2.76	2.55	2.61	2.74	2.77	2.95	3.85	3.44	2.98	2.41	2.46	3.15
Tb, ppm		0.59	0.56	0.52	0.51	0.51	0.56	0.49	0.44	0.64	0.54	0.56	0.51	0.59
Dy, ppm		3.64	3.29	3.89	3.28	3.67	3.71	4.47	3.30	3.96	4.09	3.47	3.33	3.52
Ho, ppm		0.75	0.78	0.62	0.63	0.74	0.74	0.65		0.81	0.91	0.75	0.67	0.66
Er, ppm		2.05	2.20	2.01	1.89	2.08	1.98	1.85	2.00	2.64	2.09	2.61	2.00	2.16
Tm, ppm		0.29	0.29	0.25	0.30	0.30	0.25	0.38	0.28	0.34	0.32	0.33	0.25	0.24
Yb, ppm		2.88	1.94	2.10	1.72	1.83	1.92	1.79	1.79	2.29	1.80	2.40	1.83	1.98
Lu, ppm		0.28	0.30	0.26	0.23	0.31	0.35	0.22	0.28	0.31	0.30	0.32	0.26	0.28
Hf, ppm		1.63	1.24	0.98	1.28	0.84	1.02	1.31	1.27	1.44	1.16	0.93	1.43	1.22
Pb, ppm		0.20	0.12		0.59	0.11			0.05	0.10	0.09	0.36	0.40	0.16
Th, ppm		0.03	0.03	0.02	0.04	0.02	0.01		0.02	0.03	0.02			0.02

Table DR3. Calculated* compositions and temperatures of the Gorgona komatiite melts

SAMP_NO	SiO_2	TiO_2	Al_2O_3	Fe_2O_3	FeO	MnO	MgO	CaO	Na_2O	K_2O	P_2O_5	Cr_2O_3	T_calc	Fo_host
m1 94-28_1	46.67	0.73	13.22	1.38	9.56	0.11	15.02	11.59	1.63	0.03	0.05	n.d.	1352	90.47
m1 94-28_2	46.25	0.71	13.00	1.38	9.56	0.15	15.45	11.84	1.58	0.03	0.05	n.d.	1362	90.81
m1 94-28_3a	46.53	0.69	12.98	1.38	9.57	0.17	15.65	11.37	1.59	0.03	0.05	n.d.	1365	90.83
m1 94-28_3b	46.42	0.67	12.54	1.38	9.56	0.11	16.37	11.42	1.45	0.03	0.05	n.d.	1378	91.23
m1 94-28_4a	46.52	0.66	12.41	1.38	9.56	0.14	16.78	10.96	1.52	0.02	0.05	n.d.	1386	91.4
m1 94-28_6	46.58	0.71	12.94	1.38	9.56	0.14	15.36	11.71	1.54	0.03	0.05	n.d.	1358	90.68
m1 94-28_7	46.21	0.69	13.06	1.38	9.56	0.14	15.83	11.43	1.62	0.02	0.06	n.d.	1370	91
m1 94-28_8a	46.74	0.71	12.93	1.38	9.56	0.14	15.31	11.64	1.52	0.03	0.05	n.d.	1357	90.61
m1 94-28_9a	46.58	0.72	12.99	1.38	9.56	0.13	15.39	11.66	1.52	0.03	0.05	n.d.	1359	90.69
m2 94-17_10	47.07	0.71	13.15	1.38	9.56	0.12	14.51	11.90	1.53	0.03	0.05	n.d.	1339	90.07
m2 94-17_11	47.12	0.73	13.11	1.38	9.56	0.12	14.40	12.04	1.50	0.03	0.03	n.d.	1337	90
m2 94-17_12	47.47	0.71	13.04	1.38	9.56	0.12	14.38	11.71	1.57	0.03	0.03	n.d.	1337	89.92
m2 94-17_13	46.89	0.73	13.22	1.38	9.56	0.15	14.59	11.79	1.64	0.03	0.04	n.d.	1343	90.18
m2 94-17_14	46.82	0.74	13.37	1.38	9.56	0.13	14.09	12.23	1.61	0.03	0.04	n.d.	1332	89.88
m2 94-17_15	47.36	0.74	13.63	1.38	9.56	0.14	13.27	12.19	1.65	0.04	0.04	n.d.	1314	89.18
m2 94-17_16	47.45	0.73	13.35	1.38	9.56	0.15	13.80	11.93	1.59	0.03	0.04	n.d.	1325	89.53
m2 94-17_17	47.57	0.73	13.37	1.38	9.57	0.10	13.66	11.93	1.61	0.03	0.04	n.d.	1322	89.41
m2 94-17_18	47.34	0.72	13.43	1.38	9.56	0.13	13.94	11.80	1.62	0.03	0.05	n.d.	1328	89.64
m2 94-17_18b	47.51	0.73	13.68	1.38	9.56	0.13	13.14	12.14	1.65	0.04	0.05	n.d.	1311	89.04
m3 94-4_19	47.02	0.67	12.73	1.38	9.56	0.12	15.84	11.10	1.51	0.03	0.04	n.d.	1367	90.83
m3 94-4_20	47.28	0.71	12.93	1.38	9.56	0.10	14.92	11.56	1.49	0.03	0.05	n.d.	1347	90.27
m3 94-4_21	47.04	0.70	12.79	1.38	9.56	0.10	15.43	11.43	1.49	0.03	0.05	n.d.	1358	90.61
m3 94-4_22	47.17	0.68	12.71	1.38	9.56	0.12	15.53	11.32	1.46	0.03	0.04	n.d.	1359	90.63
m3 94-4_23	47.39	0.67	12.40	1.38	9.56	0.13	15.69	11.28	1.43	0.02	0.05	n.d.	1362	90.68
m3 94-44_24	47.20	0.69	12.09	1.38	9.56	0.09	16.30	11.19	1.42	0.03	0.04	n.d.	1375	91.06
m3 94-44_25	47.53	0.70	12.55	1.38	9.56	0.10	15.26	11.38	1.47	0.03	0.04	n.d.	1354	90.43
m3 94-44_26	47.20	0.68	12.60	1.38	9.56	0.11	15.71	11.13	1.54	0.03	0.05	n.d.	1365	90.74
m3 94-44_27	47.25	0.68	12.38	1.38	9.56	0.11	15.95	11.19	1.43	0.03	0.04	n.d.	1368	90.85
m4 94-3_28	47.05	0.72	13.23	1.38	9.56	0.11	14.84	11.42	1.61	0.03	0.04	n.d.	1348	90.27
m4 94-3_29	46.85	0.68	12.95	1.38	9.56	0.10	15.95	10.92	1.54	0.02	0.05	n.d.	1369	90.9
m4 94-3_30	46.43	0.68	12.70	1.38	9.56	0.13	16.57	10.94	1.53	0.03	0.04	n.d.	1383	91.31
m4 94-3_31	46.50	0.69	12.84	1.38	9.56	0.11	16.25	11.08	1.52	0.02	0.05	n.d.	1376	91.13
m4 94-3_32	46.65	0.71	13.16	1.38	9.56	0.13	15.28	11.45	1.62	0.03	0.04	n.d.	1358	90.61
m4 94-3_33	46.84	0.68	12.64	1.38	9.56	0.11	16.25	10.94	1.54	0.02	0.04	n.d.	1376	91.08
m4 94-3_34	46.52	0.67	12.90	1.38	9.56	0.14	16.09	11.14	1.53	0.02	0.04	n.d.	1373	91.05
m4 94-3_345	46.57	0.67	12.81	1.38	9.56	0.11	16.64	10.66	1.52	0.03	0.06	n.d.	1383	91.29

m4 94-28_36	46.58	0.72	13.17	1.38	9.56	0.14	15.04	11.77	1.57	0.03	0.05	n.d.	1352	90.49
94-44 -gr1	46.73	0.68	12.32	1.38	9.56	0.11	16.39	11.25	1.28	0.02	0.07	0.22	1374	91.11
94-44-gr2	46.85	0.68	12.57	1.38	9.56	0.15	15.87	11.34	1.32	0.03	0.06	0.20	1364	90.82
94-44-gr3	46.44	0.64	12.21	1.38	9.56	0.16	17.06	11.02	1.26	0.02	0.06	0.20	1387	91.48
94-44-gr4	46.91	0.66	12.33	1.38	9.56	0.09	15.66	11.94	1.29	0.03	0.03	0.12	1361	90.77
94-44-gr5	46.54	0.64	12.26	1.38	9.56	0.10	17.07	10.98	1.30	0.02	0.04	0.11	1388	91.49
94-28-gr6	46.48	0.71	13.28	1.38	9.56	0.15	14.71	12.15	1.40	0.02	0.03	0.14	1342	90.27
94-28-gr7a	46.47	0.69	12.93	1.38	9.56	0.19	15.71	11.44	1.47	0.04	0.04	0.08	1364	90.85
94-28-gr8	46.44	0.66	12.83	1.38	9.56	0.17	16.28	11.10	1.44	0.02	0.04	0.08	1375	91.13
94-28-gr9a	46.44	0.67	12.80	1.38	9.56	0.15	15.93	11.49	1.40	0.02	0.06	0.08	1367	90.96
94-28-gr9b	46.26	0.71	12.75	1.38	9.56	0.16	15.84	11.78	1.36	0.03	0.06	0.09	1366	90.96
94-28-gr10	46.97	0.68	12.94	1.38	9.57	0.15	15.49	11.20	1.45	0.03	0.06	0.09	1358	90.6
94-28-gr11a	46.45	0.68	12.67	1.38	9.56	0.15	16.46	11.02	1.44	0.02	0.07	0.10	1378	91.21
94-28-gr11b	46.65	0.68	12.49	1.38	9.56	0.10	16.49	10.99	1.47	0.02	0.06	0.10	1379	91.21
94-28-gr12	46.88	0.64	12.65	1.38	9.56	0.14	16.24	10.90	1.43	0.02	0.07	0.10	1372	91.01
94-28-gr13	46.75	0.73	13.16	1.38	9.56	0.10	15.39	11.28	1.51	0.03	0.05	0.06	1357	90.61
Grg1 1-1	46.21	0.70	13.11	1.38	9.56	0.14	15.97	11.25	1.50	0.02	0.04	0.12	1370	91.02
Grg1 2-1	46.37	0.71	13.41	1.38	9.57	0.10	15.18	11.53	1.57	0.02	0.04	0.14	1354	90.57
Grg1 3-1	46.47	0.67	13.07	1.38	9.56	0.10	15.54	11.53	1.48	0.02	0.03	0.14	1361	90.76
Grg1 5-1	46.35	0.65	12.98	1.38	9.56	0.12	16.13	11.16	1.47	0.02	0.05	0.12	1372	91.07
Grg1 6-1	46.72	0.67	13.18	1.38	9.56	0.14	14.97	11.65	1.51	0.03	0.08	0.12	1348	90.37
Grg1 7-1	46.17	0.69	12.86	1.38	9.56	0.13	16.38	11.19	1.45	0.04	0.02	0.14	1378	91.24
Grg1 8a-1	46.23	0.71	12.98	1.38	9.56	0.12	15.84	11.53	1.45	0.02	0.06	0.13	1367	90.96
Grg1 8b-2	45.75	0.66	13.09	1.38	9.56	0.11	16.59	11.24	1.40	0.02	0.05	0.15	1381	91.39
Grg2 1-1	46.44	0.68	13.06	1.38	9.56	0.10	15.43	11.65	1.50	0.03	0.07	0.11	1359	90.71
Grg2 2-1	46.37	0.68	12.91	1.38	9.56	0.13	16.12	11.22	1.41	0.02	0.04	0.15	1371	91.05
Grg2 3-1	46.29	0.72	13.20	1.38	9.56	0.10	15.50	11.59	1.46	0.03	0.04	0.13	1360	90.76
Grg2 4-1	46.59	0.70	13.05	1.38	9.56	0.15	15.33	11.55	1.49	0.03	0.06	0.12	1356	90.61
Grg2 5-1	46.51	0.68	13.16	1.38	9.56	0.11	15.23	11.70	1.48	0.04	0.05	0.12	1354	90.58
Grg2 7-1	46.42	0.67	12.74	1.38	9.56	0.11	16.20	11.24	1.46	0.02	0.08	0.13	1373	91.1
Grg2 8-1	46.57	0.68	12.88	1.38	9.56	0.13	15.91	11.21	1.47	0.02	0.06	0.13	1367	90.92
Grg3 1-1	46.70	0.73	13.39	1.38	9.56	0.12	14.54	11.87	1.53	0.03	0.04	0.11	1340	90.13
Grg3 4-1	46.34	0.65	13.04	1.38	9.56	0.13	15.93	11.35	1.43	0.03	0.05	0.13	1367	90.96
Grg3 5-1	46.46	0.66	13.12	1.38	9.56	0.13	15.39	11.65	1.48	0.03	0.03	0.12	1358	90.68

* Calculation, using the model by Ford et al. (1983) and PETROLOG software by L. Danyushevsky (2001), was based on the compositions of heated melt inclusions (see Table DR2), corrected for "Fe-loss", their host olivine and melt's FeO = 10.8 and Fe^{2+}/Fe^{3+} = 7.7)
The total FeO in the melt was assumed to be equal to the average FeO in the whole rocks.
The degree of Fe oxidation in the melt was calculated using Fe2+/Fe3+ of Cr-spinel and empirical model of Maurel and Maurel (1982).

References:

Danyushevsky, L.V., 2001, The effect of small amounts of H_2O on crystallisation of mid-ocean ridge and backarc basin magmas: Journal of Volcanology and Geothermal Research, v. 110, p. 265–280

Ford, C.E., Russel, D.G., Craven, J.A., and Fisk, M.R., 1983, Olivine-liquid equilibria: temperature, pressure and composition dependence of the crystal/liquid cation partition coefficients for Mg, Fe^{2+}: Ca and Mn: Journal of Petrology, v. 24, p. 256–265.

Maurel, C., and Maurel, P., 1982, Etude expérimentale de l'équilibre Fe2+-Fe3+ dans les spinelles chromifères et les liquides silicates basiques coexistants, à 1 atm: Comptes Rendus de l'Academie des Sciences (Paris), v. 295, p. 209-212.

References:

Chaussidon, M., and Libourel, G., 1993, Boron partitioning in the upper mantle: an experimental and ion probe study: Geochimica et Cosmochimica Acta, v. 57, p. 5053-5062.

Dixon, J.E., Clague, D.A., and Stolper, E.M., 1991, Degassing history of water, sulfur and carbon in submarine lavas from Kilauea volcano, Hawaii: Journal of Geology, v. 99, p. 371-394.

Fahey, A.J., Zinner, E.K., Crozaz, G., and Kornacki, A.S., 1987, Microdistributions of Mg isotopes and REE abundances in a Type A calcium-aluminum-rich inclusion from Efremovka: Geochimica Et Cosmochimica Acta, v. 51, p. 3215-3229.

Jarosewich, E.J., Nelen, J.A., and Norberg, J.A., 1980, Reference samples for electron microprobe analysis: Geostandards Newsletter, v. 4, p. 43-47.

Jochum, K.P., Dingwell, D.B., Rocholl, A., Stoll, B., Hofmann, A.W., Becker, S., Besmehn, A., Bessette, D., Dietze, H.J., Dulski, P., Erzinger, J., Hellebrand, E., Hoppe, P., Horn, I., Janssens, K., Jenner, G.A., Klein, M., McDonough, W.F., Maetz, M., Mezger, K., Munker, C., Nikogosian, I.K., Pickhardt, C., Raczek, I., Rhede, D., Seufert, H.M., Simakin, S.G., Sobolev, A.V., Spettel, B., Straub, S., Vincze, L., Wallianos, A., Weckwerth, G., Weyer, S., Wolf, D., and Zimmer, M., 2000, The preparation and preliminary characterisation of eight geological MPI-DING reference glasses for in-site microanalysis: Geostandards Newsletter-the Journal of Geostandards and Geoanalysis, v. 24, p. 87-133.

Longerich, H.P., Jackson, S.E., and Gunther, D., 1996, Laser ablation inductively coupled plasma mass spectrometric transient signal data acquisition and analyte concentration calculation: Journal of Analytical Atomic Spectrometry, v. 11, p. 899-904.

Pearce, N.J.G., Perkins, W.T., Westgate, J.A., Gorton, M.P., Jackson, S.E., Neal, C.R., and Chenery, S.P., 1997, A compilation of new and published major and trace element data for NIST SRM 610 and NIST SRM 612 glass reference materials: Geostandards Newsletter-the Journal of Geostandards and Geoanalysis, v. 21, p. 115-144.

Sobolev, A.V., and Chaussidon, M., 1996, H_2O concentrations in primary melts from supra-subduction zones and mid-ocean ridges: Implications for H_2O storage and recycling in the mantle: Earth and Planetary Science Letters, v. 137, p. 45-55.

Thordarson, T., Self, S., Oskarsson, N., and Hulsebosch, T., 1996, Sulfur, chlorine, and fluorine degassing and atmospheric loading by the 1783-1784 AD Laki (Skaftar Fires) eruption in Iceland: Bulletin of Volcanology, v. 58, p. 205-225.

Zinner, E., and Crozaz, G., 1986, A method for the quantitative measurement of rare earth elements in the ion microprobe: International Journal of Mass Spectrometry and Ion Processes, v. 69, p. 17-38.